All-silicon interferometer with multimode waveguides for temperature-insensitive filters and compact biosensors

Guan, Xiaowei; Frandsen, Lars Hagedorn

Published in:
Optics Express

Link to article, DOI:
10.1364/OE.27.000753

Publication date:
2019

Document Version
Publisher's PDF, also known as Version of record

Research Article | Vol. 27, No. 2 | 21 Jan 2019 | OPTICS EXPRESS 753
Optics EXPRESS

All-silicon interferometer with multimode waveguides for temperature-insensitive filters and compact biosensors

XIAOWEI GUAN* AND LARS H. FRANDSEN

DTU Fotonik, Department of Photonics Engineering, Technical University of Denmark, 2800 Kgs. Lyngby, Denmark
**xgua@fotonik.dtu.dk*

Abstract: We report a novel design of an all-silicon temperature-independent filter employing a Mach-Zehnder interferometer (MZI) with multimode waveguides. The two arms of the MZI have equal lengths and equal widths but propagate different modes having different effective indices to guarantee an optical path difference (OPD) but similar temperature-dependence to diminish any thermal shifts of the interference pattern. A temperature-independent MZI filter with only one channel is also proposed and experimentally demonstrated. Measurements verify the principle of operation and a low temperature sensitivity of –20 to 10 pm/°C in the C-band for both MZI filters is achieved. The one-channel MZI structure is furthermore employed to achieve a compact sensor exhibiting a high sensitivity of 826 nm/RIU (refractive index unit).

1. Introduction

Silicon photonics is foreseen as a promising platform for emerging technologies within quantum communication [1,2] and artificial intelligence [3,4], and is taking a vital role on optical interconnects dealing with ultra-dense data [5–8] and biosensors for label-free detection [9–12]. The arguments for silicon photonic devices are mainly addressing their compactness and resemblance to silicon electronic integrated circuits (ICs) in terms of fabrication. However, there are yet some challenges hindering silicon photonic devices for broader practical implementations, among which a large thermal drift is detrimental to the performances of silicon photonic devices due to the inherently large thermo-optic coefficient (TOC) of silicon (1.86×10^{-4}/°C [13]). For example, the two arms of a Mach-Zehnder interferometer (MZI)-based biosensor has to be approximately identical to cancel out the influence of thermal fluctuations but, therefore, the arms need to be very long (2 mm) to achieve enough phase shifts [14], challenging the practical integration of such with ICs.

To overcome the influence of thermal fluctuations on a silicon photonic chip, it is natural to use thermo-electric coolers (TEC) to externally stabilize the chip temperature or to use on-chip heaters to locally compensate the temperature drift [15–17]. Nevertheless, both methods are dramatically increasing the complexity and the power consumption of the system. Alternatively, athermal schemes have been developed by covering the silicon photonic devices with negative TOC materials [18–22] or by using all-silicon asymmetric MZI to cancel out the thermal drift [23–26]. The first scheme will impose additional steps on the fabrication by cladding the silicon waveguides with e.g. polymers or titanium dioxide possessing a negative TOC, as well as inevitably employing narrow silicon waveguides with a larger loss [21] to increase the overlap of the mode with the negative TOC material. The all-silicon scheme typically involves the use of an asymmetric MZI structure, in which the two arms are designed to have either different widths [23–25], different modes [26,27] or even different waveguide configurations [28,29] to balance out temperature effects, which will

#348374 https://doi.org/10.1364/OE.27.000753
Journal © 2019 Received 16 Oct 2018; revised 6 Dec 2018; accepted 11 Dec 2018; published 9 Jan 2019

Optics EXPRESS

restrict the design flexibility and limit the use of such especially for athermal filters with different free-spectral ranges (FSRs).

Here, we propose and experimentally demonstrate a novel temperature-insensitive all-silicon MZI having two waveguide arms of equal length and width. The design is based on the finding that a lower-order mode and a higher-order mode can experience an equal phase shift with respect to a change in temperature in a silicon multimode waveguide at specific critical width. If both arms of equal lengths of the MZI are designed with the critical width and separately propagate the lower- and higher-order modes, the MZI can achieve very low temperature sensitivity. The lengths of the arms will not be restricted but only depend on the desired FSRs. Recently, we presented such a design concept in our previous conference abstract [30]. In this paper, we will elucidate details of the design principle and - more importantly - we will experimentally verify the superiority of adjusting the arm lengths to achieve the desired FSRs while sustaining the athermal capability. Furthermore, as both arms are of equal lengths and widths, the present MZI can be designed to have only one channel. The one-channel MZI decreases the device area footprint and combining the two channels as a single one will mitigate sufferings from the more or less non-uniformity of the SOI wafer or the particles generating in the fabrication, in case they occur as an issue. Although one-channel interferometers employing multimode waveguides have already been theoretically [31] and experimentally [32,33] demonstrated for biomedical sensors, the coupling of light to the different modes are realized by offsetting the input waveguide, which may limit the design in only using few modes. Here, our one-channel MZI are realized by employing adiabatic tapers and directional couplers (DCs) exhibiting greater design flexibilities. Both of our two-channel and one-channel MZI temperature-insensitive filters can achieve a small temperature sensitivity of –20 to 10 pm/°C for the whole C-band, comparable with the previous results of <8 pm/K in a wavelength range of 30 nm [27]. Moreover, we demonstrate a biomedical sensor based on the one-channel MZI having sensitivity as large as 826 nm/RIU.

2. Structure and design

We used an eigenmode solver (Mode Solution from Lumerical Inc.) to calculate the effective indices (n_{eff}, solid lines) and the temperature dependences ($\mathrm{d}n_{\mathrm{eff}}/\mathrm{d}T$, dashed lines) for transverse-electric (TE) modes of different orders with respect to the waveguide width w of a silicon waveguide of height h = 250 nm buried in silica (SiO_2), as shown in Fig. 1. In the calculations, TOCs and refractive indices at the wavelength of 1550 nm are chosen as 1.86 x 10^{-4}/°C and 3.455 for silicon, and 0.08 x 10^{-4}/°C and 1.445 for SiO_2, respectively. For any width of a multimode waveguide, the higher-order mode will always have a smaller n_{eff} than the lower-order mode, due to a weaker confinement in the higher-index core. However, the $\mathrm{d}n_{\mathrm{eff}}/\mathrm{d}T$ curves may cross at some critical width. For smaller w, $\mathrm{d}n_{\mathrm{eff}}/\mathrm{d}T$ increases rapidly with w since it is dominated by large changes in the mode confinement [34]. For larger w, $\mathrm{d}n_{\mathrm{eff}}/\mathrm{d}T$ decreases slowly with a factor w^{-2} since the absolute value of n_{eff} dominates and decreases with w^{-2} [23]. Due to a weaker confinement of the higher-order modes, the curves of $\mathrm{d}n_{\mathrm{eff}}/\mathrm{d}T$ versus w are moved towards larger w compared to that of the lower-order modes. Thus, the lower-order mode and the higher-order mode will cross at a critical width, where they have different effective indices but the equal temperature dependences of the refractive indices. For example, the critical width w_c for the TE_0 mode and the TE_1 mode is 623 nm, where $\mathrm{d}n_{\mathrm{eff}}/\mathrm{d}T$ of both modes is 1.993 x 10^{-4}/°C with effective indices Δn_{eff} of 0.8246. In the following, we use the TE_0 mode and the TE_1 mode and choose w_c = 623 nm as the widths for both arms of our temperature-insensitive MZI (TI-MZI).

Optics EXPRESS

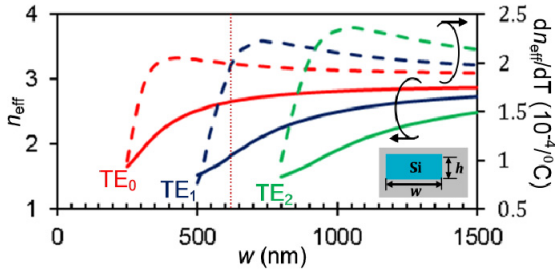

Fig. 1. (a) Calculated effective indices (solid lines) and temperature dependences (dashed lines) for the TE_0 (red), TE_1 (blue), and TE_2 (green) modes at 1550 nm in a silicon waveguide (shown in the inset) of height h = 250 nm buried in SiO_2. The dotted line indicates the critical width for the TE_0 mode and the TE_1 mode.

Figure 2(a) schematically illustrates the configuration of the proposed TI-MZI with two channels. The fundamental TE_0 mode at 1550 nm inputted from the 450nm-wide single-mode waveguide is equally split into two parts by the first symmetric directional coupler (DC). The upper part is coupled to the TE_0 mode in the 623 nm-wide multimode waveguide of arm 2 by using an adiabatic taper with a length of 5 μm. The lower part is firstly coupled to the TE_0 mode in a narrow waveguide by an adiabatic taper with length 5 μm and subsequently coupled to the TE_1 mode in the 623nm-wide waveguide of arm 1 by an asymmetric DC (ADC). Finally, the TE_0 mode in arm 2 and the TE_1 mode in arm 1 are separately coupled back to the TE_0 mode in the 450nm-wide waveguide after propagating along the arms with a length of L, and interfere in the last symmetric DC. Since the two arms have the equal widths w_c and the equal lengths L, the two-channel TI-MZI can be easily adjusted to have only one channel as shown in Fig. 2(b). The widths of the narrow waveguides are chosen to w_{narrow} = 288 nm to achieve phase matching between the TE_0 mode and the TE_1 mode in the 623nm-wide multimode waveguide. Figure 2(c) shows the calculated and normalized (to a straight waveguide) transmissions of the asymmetric DC which converts the TE_0 mode in the 288nm-wide single-mode waveguide to the TE_1 mode in the 623nm-wide multimode waveguide as shown in the inset. The conversion efficiency is ~98% at 1550 nm resulting in an extinction ratio (ER) of ~21 dB between transmissions in the cross port and the thru port.

The TI-MZI contains different connecting waveguide sections with lengths L' (Fig. 2), which are not completely symmetric with this asymmetry being much pronounced for the one-channel design. This will possibly introduce differences in the accumulated dn_{eff}/dT for the two arms. However, the influence of the different sections can be negligible if L>>L' according to the formula for the temperature sensitivity S of the TI-MZI,

$$S = \frac{\Delta\lambda}{\Delta T} = \lambda \frac{(dn_{neff}^{TE0}/dT - dn_{neff}^{TE1}/dT)\cdot L + \Delta(dn'_{eff}/dT)\cdot 2\cdot L'}{\Delta n_g \cdot L + \Delta n'_g \cdot 2 \cdot L'}. \quad (1)$$

Here, λ is the interference wavelength and Δn_g is the group index difference between the two modes in the multimode waveguide, i.e. 0.566 in the case for TE_0 and TE_1. Δn_g' and $\Delta(dn_{eff}'/dT)$ are the group index difference and the difference in temperature dependence of the effective indices of the upper and lower connecting waveguide sections averaged over L', respectively. The first part in the numerator will be always zero since the two modes have the same temperature dependence and for L>>L', S goes to zero.

Optics EXPRESS

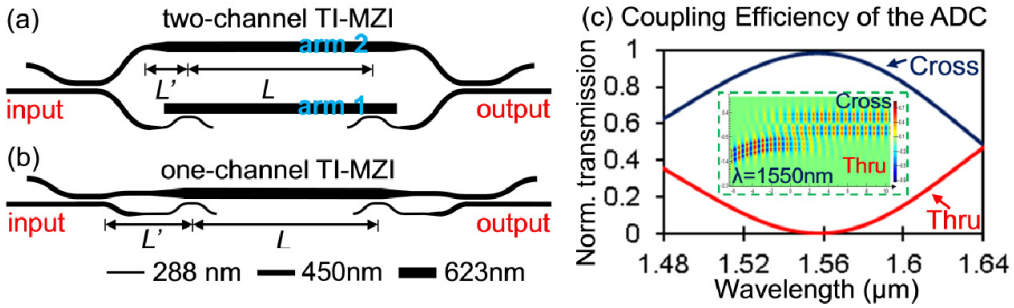

Fig. 2. Schematic of the proposed TI-MZI with two channels (a) and one channel (b). (c) Calculated and normalized transmissions for the designed asymmetric DC with the inset showing light propagation of the asymmetric DC at 1550 nm.

3. Fabrication and characterization

The designed TI-MZIs are fabricated on a silicon-on-insulator (SOI) chip having a 250-nm top silicon layer on a 3-μm thick silica layer. A positive resist ZEP520A is spun on the chip and patterned using electron beam lithography to act as a soft mask in an inductively coupled plasma (ICP) etching machine using sulfur hexafluoride (SF_6) and octafluorocyclobutane (C_4F_8) gases to etch the silicon. The etching is utilizing a Bosch process having alternations between an etch cycle (5 seconds) and a passivation cycle (3 seconds) with the platen temperature cooled down to 10 °C. The residual resist is stripped and the chip is covered with a 1-μm thick layer of silica. Optical microscope images of the fabricated two-channel and one-channel TI-MZIs are shown in Figs. 3(a) and 3(b), respectively. On-chip grating couplers (GCs) are used for coupling light to and from the chip [35]. Insets framed in green and red in Fig. 3(a) show scanning electron microscopy (SEM) images of the adiabatic taper (red) and the mode coupler (green). The SEM image in Fig. 3(b) shows the connecting part including the 50%:50% splitter, the adiabatic tapers and the mode coupler of the one-channel MZI.

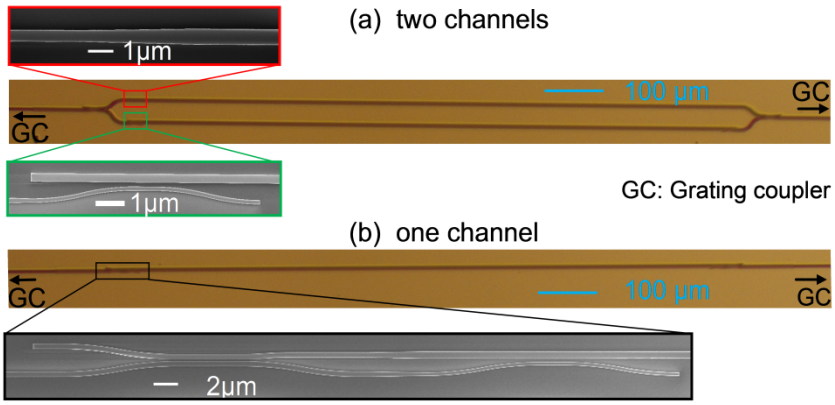

Fig. 3. Microscope images of the fabricated (a) two-channel and (b) one-channel TI-MZI with the inserted SEM images showing the connecting parts. The stair-casings in the curved parts of the SEM images are due to the low zoom used when scanning a large area.

To verify the temperature-insensitivity of the fabricated MZIs, we have characterized the MZIs at different temperatures and normalized the recorded transmission spectra to the transmission of a straight waveguide at the corresponding temperatures to cancel out any temperature-dependence of the grating couplers. The normalized transmission spectra are shown in Fig. 4(a) for a two-channel TI-MZI with L = 1.097 mm, Fig. 4(b) for a two-channel TI-MZI with L = 0.276 mm, and Fig. 4(c) for a one-channel TI-MZI with L = 1.097 mm. The

Optics EXPRESS

measured spectra have been fitted by trigonometric curves to get the exact destructive wavelengths but not shown in the figures. At 1550 nm, insertion losses of the 0.276mm-long and the 1.097mm-long two-channel filters are measured to ~0.1 dB and ~1.6 dB. The one-channel TI-MZI filter shows a low loss of ~0.7 dB with an ER ~11 dB around 1550 nm. Figure 4(d) shows the temperature sensitivity as a function of wavelength for all MZI configurations and we find temperature-dependent wavelength shifts lower than 1 pm/°C at 1547 nm for the two-channel and the one-channel MZI having the longer arm. In the whole C-band (1535 nm – 1565 nm) the wavelength shift stays between −20 to 10 pm/°C. The wavelength for achieving zero thermal drift for the shorter two-channel filter moves to around 1535 nm since the two connecting parts introduce a relative higher temperature dependence of the filter. Nevertheless, the shorter filter can still achieve a temperature-dependent wavelength shift lower than 10 pm/°C in 20 nm wavelength region from 1525 nm to 1545 nm. Furthermore, we find the FSR of the shorter MZI (13.14 nm) to be ~3.6 times larger than that of the longer MZI's (3.67 nm), which illustrates the flexibility in the design of the TI-MZI filters with different bandwidths.

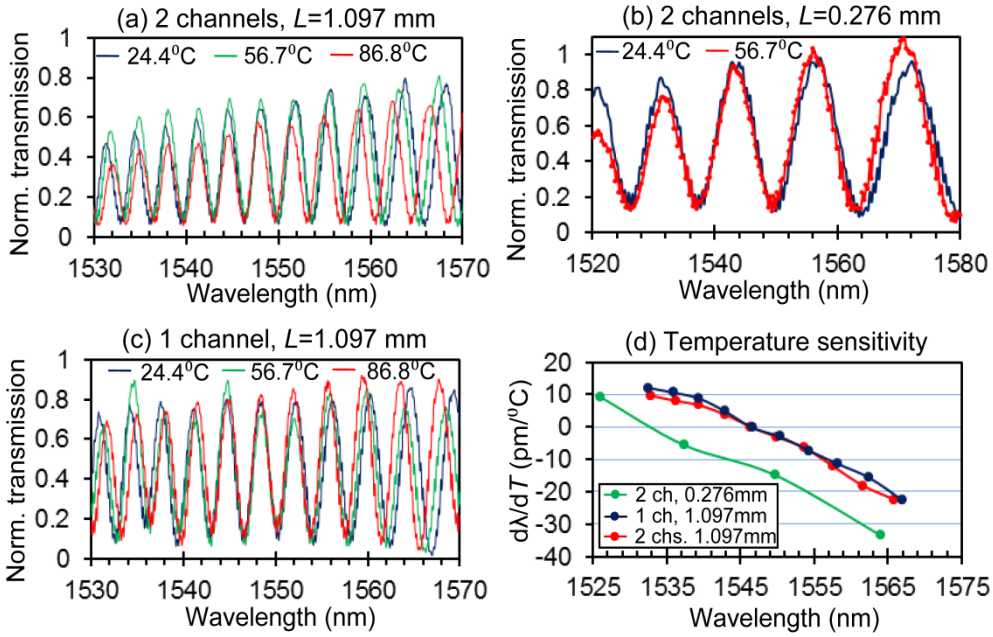

Fig. 4. Measured and normalized transmission spectra at different temperatures for (a) the two-channel TI-MZI filter with L = 1.097 mm, (b) the two-channel TI-MZI filter with L = 0.276 mm, and (c) the one-channel TI-MZI filter with L = 1.097 mm. (d) The temperature sensitivity as a function of wavelength for the above filters with points showing the destructive interference wavelengths.

The proposed one-channel MZI is applied as a compact biosensor utilizing the different responses to a change in the top cladding index of the modes in the multimode waveguide. We selectively open a window in the top cladding on the waveguide channel in the one-channel filter with L = 1.097 mm by etching the top silica cladding with a 5% hydrofluoric (HF) acid solution. Figure 5(a) shows a microscopy image of the fabricated sensor. The dependency of the effective indices of the modes at different waveguide widths on the refractive index of the analyte (dn_{eff}/dn_c) flowing into the opened window are calculated and shown in Fig. 5(b) with the waveguide cross section illustrated in the inset. Here, the wavelength is 1550 nm and the waveguide height is 250 nm. The higher-order TE_1 mode has a larger dn_{eff}/dn_c due to a weaker mode confinement and, hence, a larger overlap with the

Optics EXPRESS

analyte. For a width of 623 nm (indicated by the vertical brown dotted line in Fig. 5(b)) the $\Delta(dn_{eff}/dn_c)$ between the TE_0 mode and the TE_1 mode is as large as 0.35, suggesting a large sensitivity of the sensor. We separately drop deionized (DI) water and a phosphide buffer solution (PBS) with different concentrations onto the sample and measure the transmission spectra of the sensor. Figure 5(c) shows the normalized measured spectra of the sensor when the sample is covered by DI water (black), 0.25x PBS (red), 0.5x PBS (green), 0.75x PBS (light blue), and 1x PBS (dark blue). Here, the standard 1x PBS was diluted with 3/1/0.33 times volume of DI water to achieve the 0.25x/0.5x/0.75x PBS, respectively. The ripples on the transmission spectra are caused by Fabry-Perot cavities formed between the waveguide couplers and the sensing window boards. Trigonometric curves are used to fit the measured spectra to extract the exact destructive interference wavelengths (not shown in the figure). The transmission spectra are found to red shift as the PBS concentration increases while the insertion loss of the sensor stays around 1.8 dB. Figure 5(d) plots the wavelength shift of the sensor compared to the case of applying DI water with respect to the refractive index change of the PBS at different concentrations. Here, as the concentration increases, the refractive index of the PBS linearly increases with a rate of ~0.005 per 3x [36]. The linear fitting yields a sensitivity, $\Delta\lambda/\Delta n_c$, of 826 nm/RIU (refractive index unit). It is noted that the sensitivity of the present refractive index sensor is one order larger than that of a traditional silicon single-mode waveguide sensor (70 nm/RIU [9]) since by leveraging the higher-order mode light can be more effectively overlapped with the cladding analytes. The sensitivity S can also be calculated by $S = \lambda(\Delta dn_{eff}/dn_c)/\Delta n_g$ and a value of 728 nm/RIU is derived. Here, $\Delta dn_{eff}/dn_c$ and Δn_g are differences of dn_{eff}/dn_c and group indices between the two modes (TE_0 and TE_1), respectively, and $\lambda = 1550$ nm. A larger measured sensitivity can be attributed to an undercut of the silica beneath the waveguide in the HF etch. It is worth to note that the proposed biosensor design can be shortened while keeping a high sensitivity as the sensitivity S is independent on the arm length.

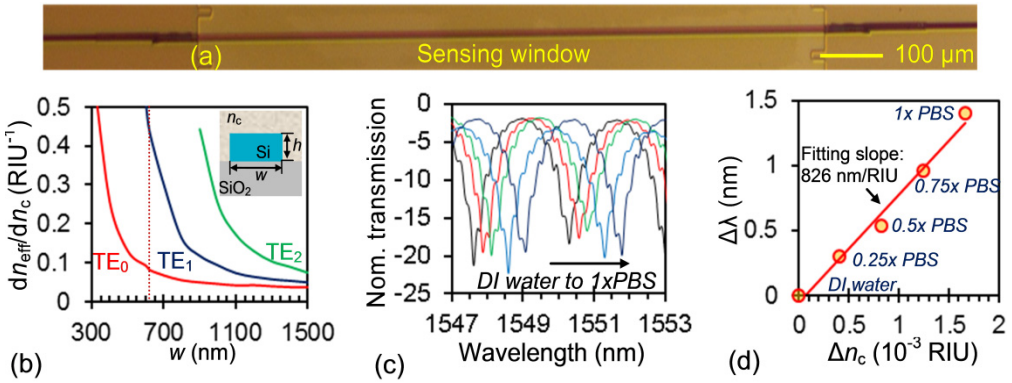

Fig. 5. (a) Microscopy image of the one-channel MZI biosensor. (b) Calculated change of the effective mode index on the refractive index of the cladding analyte (n_c) for different modes as a function of the waveguide width. Inset shows the cross section of the waveguide. Here, the wavelength is 1550 nm and h = 250 nm. The vertical dotted line indicates where w = 623 nm. (c) Measured and normalized transmission spectra and (d) the destructive interference wavelength shift of the biosensor immersed in DI water (black) or PBS with concentrations of 0.25x (red), 0.5x (green), 0.75x (light blue) and 1x (dark blue).

4. Conclusion

We have proposed and experimentally demonstrated a novel design of an all-silicon Mach-Zehnder interferometer with low sensitivity to temperature changes having two multimode waveguide channels of equal widths and lengths and, thus, being able to be adjusted to a more compact one-channel interferometer. The principle of operation is based on transmitting two different modes in a silicon multimode waveguide, which can have equal temperature

Optics EXPRESS

dependence of the phase shift at a critical waveguide width. By choosing the waveguide width to 623 nm applicable for the TE_0 and the TE_1 mode, we have fabricated and measured the MZI filters and found that both the two-channel filter and the one-channel filter can achieve a low thermal drift in the range from −20 to 10 pm/°C in the C-band while exhibiting a low insertion loss of 1.6 dB for the two-channel interferometer and 0.7 dB for the one-channel interferometer. Measurements on the interferometers with different arm lengths show the design flexibility to achieve different free-spectral-ranges while keeping the athermal performance. The design of the one-channel interferometers is further applied as a compact biosensor having a measured sensitivity as large as 826 nm/RIU and a low insertion loss of 1.8 dB. It should be noted that in this work we did not try to extract a thermo-optic coefficient of the PBS solutions as they quickly condense in the present device and, thus, we didn't put focus on characterizing the MZI structure as an athermal biosensor, i.e. measuring the thermal dependency of the proposed biosensor. However, the proposed concept can easily be applied for such purpose if the liquid analyte is sealed in a microfluidic channel to avoid the evaporation, hence, realizing a highly sensitive and athermal biosensor. Resembling to all other all-silicon interferometer designs, the performances of the present design will also be degraded by the fabrication errors in the waveguide width and the fabrication tolerance of the present design is calculated to be −5 to 7 nm assuming a ± 10 pm/°C offset. The present design, both for the temperature-independent filter and the compact biosensor, can be easily expanded to use even higher-order modes to keep in step with the development of the emerging mode multiplexing technologies. We believe our design strategy opens for great design flexibility, low insertion losses, and low temperature sensitivities for integrated silicon temperature insensitive filters and compact biosensors.

Funding

Det Frie Forskningsråd (Danish Council for Independent Research) (DFF-7107-00242); Villum Fonden (Villum Foundation) (VKR023112).

Acknowledgments

We thank Shu Fang and Ditte C. Andersen at the Odense University Hospital of South Denmark University (OUH, SDU) for providing the PBS solutions with different concentrations and meaningful discussions.

References

1. J. W. Silverstone, D. Bonneau, K. Ohira, N. Suzuki, H. Yoshida, N. Iizuka, M. Ezaki, C. M. Natarajan, M. G. Tanner, R. H. Hadfield, V. Zwiller, G. D. Marshall, J. G. Rarity, J. L. O'brien, and M. G. Thompson, "On-chip quantum interference between silicon photon-pair sources," Nat. Photonics **8**(2), 104–108 (2014).
2. L. T. Feng, M. Zhang, Z. Y. Zhou, M. Li, X. Xiong, L. Yu, B. S. Shi, G. P. Guo, D. X. Dai, X. F. Ren, and G. C. Guo, "On-chip coherent conversion of photonic quantum entanglement between different degrees of freedom," Nat. Commun. **7**, 11985 (2016).
3. Y. Shen, N. C. Harris, D. Englund, and M. Soljacic, "Deep learning with coherent nanophotonic circuits," Nat. Photonics **11**(7), 441–446 (2017).
4. M. J. R. Heck, J. F. Bauters, M. L. Davenport, J. K. Doylend, S. Jain, G. Kurczveil, S. Srinivasan, Y. Tang, and J. E. Bowers, "Hybrid silicon photonic integrated circuit technology," IEEE J. Quantum Electron. **19**(4), 6100117 (2013).
5. J. Wang, S. Paesani, R. Santagati, S. Knauer, A. A. Gentile, N. Wiebe, M. Petruzzella, J. L. O'brien, J. G. Rarity, A. Laing, and M. G. Thompson, "Experimental quantum Hamiltonian learning," Nat. Phys. **13**(6), 551–555 (2017).
6. B. Jalali and S. Fathpour, "Silicon Photonics," J. Lightwave Technol. **24**(12), 4600–4615 (2006).
7. C. Batten, A. Joshi, J. Orcutt, A. Khilo, B. Moss, C. W. Holzwarth, M. A. Popovic, H. Li, H. L. Smith, J. L. Hoyt, F. X. Kartner, R. J. Ram, V. Stojanović, and K. Asanović, "Building many-core processor-to-DRAM networks with monolithic CMOS silicon photonics," IEEE Micro **29**(4), 8–21 (2009).
8. C. Sun, M. T. Wade, Y. Lee, J. S. Orcutt, L. Alloatti, M. S. Georgas, A. S. Waterman, J. M. Shainline, R. R. Avizienis, S. Lin, B. R. Moss, R. Kumar, F. Pavanello, A. H. Atabaki, H. M. Cook, A. J. Ou, J. C. Leu, Y. H. Chen, K. Asanović, R. J. Ram, M. A. Popović, and V. M. Stojanović, "Single-chip microprocessor that communicates directly using light," Nature **528**(7583), 534–538 (2015).

Optics EXPRESS

9. K. De Vos, I. Bartolozzi, E. Schacht, P. Bienstman, and R. Baets, "Silicon-on-Insulator microring resonator for sensitive and label-free biosensing," Opt. Express **15**(12), 7610–7615 (2007).
10. J. Juan-Colás, A. Parkin, K. E. Dunn, M. G. Scullion, T. F. Krauss, and S. D. Johnson, "The electrophotonic silicon biosensor," Nat. Commun. **7**, 12769 (2016).
11. A. L. Washburn, M. S. Luchansky, A. L. Bowman, and R. C. Bailey, "Quantitative, label-free detection of five protein biomarkers using multiplexed arrays of silicon photonic microring resonators," Anal. Chem. **82**(1), 69–72 (2010).
12. A. L. Washburn, L. C. Gunn, and R. C. Bailey, "Label-free quantitation of a cancer biomarker in complex media using silicon photonic microring resonators," Anal. Chem. **81**(22), 9499–9506 (2009).
13. R. Dekker, N. Usechak, M. Först, and A. Driessen, "Ultrafast nonlinear all-optical processes in silicon-on-insulator waveguides," J. Phys. D Appl. Phys. **40**(14), R249–R271 (2007).
14. A. Densmore, D.-X. Xu, S. Janz, P. Waldron, T. Mischki, G. Lopinski, A. Delâge, J. Lapointe, P. Cheben, B. Lamontagne, and J. H. Schmid, "Spiral-path high-sensitivity silicon photonic wire molecular sensor with temperature-independent response," Opt. Lett. **33**(6), 596–598 (2008).
15. H. Yu, M. Pantouvaki, S. Dwivedi, P. Verheyen, G. Lepage, R. Baets, W. Bogaerts, P. Absil, and J. Van Campenhout, "Compact thermally tunable silicon racetrack modulators based on an asymmetric waveguide," IEEE Photonics Technol. Lett. **25**(2), 159–162 (2013).
16. P. Dong, W. Qian, H. Liang, R. Shafiiha, D. Feng, G. Li, J. E. Cunningham, A. V. Krishnamoorthy, and M. Asghari, "Thermally tunable silicon racetrack resonators with ultralow tuning power," Opt. Express **18**(19), 20298–20304 (2010).
17. K. Padmaraju, D. F. Logan, J. J. Ackert, A. P. Knights, and K. Bergman, "Microring resonance stabilization using thermal dithering," IEEE OI Conf., pp.58–59, 2013.
18. L. Wang, W. Bogaerts, P. Dumon, S. K. Selvaraja, J. Teng, S. Pathak, X. Han, J. Wang, X. Jian, M. Zhao, R. Baets, and G. Morthier, "Athermal arrayed waveguide gratings in silicon-on-insulator by overlaying a polymer cladding on narrowed arrayed waveguides," Appl. Opt. **51**(9), 1251–1256 (2012).
19. J. Teng, P. Dumon, W. Bogaerts, H. Zhang, X. Jian, X. Han, M. Zhao, G. Morthier, and R. Baets, "Athermal Silicon-on-insulator ring resonators by overlaying a polymer cladding on narrowed waveguides," Opt. Express **17**(17), 14627–14633 (2009).
20. S. Feng, K. Shang, J. T. Bovington, R. Wu, B. Guan, K.-T. Cheng, J. E. Bowers, and S. J. Yoo, "Athermal silicon ring resonators clad with titanium dioxide for 1.3μm wavelength operation," Opt. Express **23**(20), 25653–25660 (2015).
21. B. Guha, J. Cardenas, and M. Lipson, "Athermal silicon microring resonators with titanium oxide cladding," Opt. Express **21**(22), 26557–26563 (2013).
22. Y. Zhang and Y. Shi, "Temperature insensitive lower-index-mode photonic crystal nanobeam cavity," Opt. Lett. **40**(2), 264–267 (2015).
23. M. Uenuma and T. Moooka, "Temperature-independent silicon waveguide optical filter," Opt. Lett. **34**(5), 599–601 (2009).
24. B. Guha, A. Gondarenko, and M. Lipson, "Minimizing temperature sensitivity of silicon Mach-Zehnder interferometers," Opt. Express **18**(3), 1879–1887 (2010).
25. B. Guha, B. B. C. Kyotoku, and M. Lipson, "CMOS-compatible athermal silicon microring resonators," Opt. Express **18**(4), 3487–3493 (2010).
26. P. Xing and J. Viegas, "Broadband CMOS-compatible SOI temperature insensitive Mach-Zehnder interferometer," Opt. Express **23**(19), 24098–24107 (2015).
27. S. Dwivedi, H. D'Heer, and W. Bogaerts, "A compact all-silicon temperature insensitive filter for WDM and bio-sensing applications," IEEE Photonics Technol. Lett. **25**(22), 2167–2170 (2013).
28. P. Xing and J. Viegas, "Subwavelength grating waveguide-integrated athermal Mach-Zehnder interferometer with enhanced fabrication error tolerance and wide stable spectral range," Proc. SPIE **9752**, 97520U (2016).
29. T. Hiraki, H. Fukuda, K. Yamada, and T. Yamamoto, "Small Sensitivity to Temperature Variations of Si-Photonic Mach–Zehnder Interferometer Using Si and SiN Waveguides," Front. Mater. **2**, 1–5 (2015).
30. X. Guan and L. H. Frandsen, "All-silicon thermal independent Mach-Zehnder interferometer with multimode waveguides," IEEE International Conference on Group IV Photonics, pp. 8–9, 2016.
31. R. Levy and S. Ruschin, "Design of a single-channel modal interferometer waveguide sensor," IEEE Sens. J. **9**(2), 146–153 (2009).
32. Q. Liu, K. W. Kim, Z. Gu, J. S. Kee, and M. K. Park, "Single-channel Mach-Zehnder interferometric biochemical sensor based on two-lateral-mode spiral waveguide," Opt. Express **22**(23), 27910–27920 (2014).
33. K. E. Zinoviev, A. B. González-Guerrero, C. Domínguez, and L. M. Lechuga, "Integrated bimodal waveguide interferometric biosensor for label-free analysis," J. Lightwave Technol. **29**(13), 1926–1930 (2011).
34. W. N. Ye, J. Michel, and L. C. Kimerling, "Athermal high-index-contrast waveguide design," IEEE Photonics Technol. Lett. **20**(11), 885–887 (2008).
35. Y. Ding, H. Ou, and C. Peucheret, "Ultrahigh-efficiency apodized grating coupler using fully etched photonic crystals," Opt. Lett. **38**(15), 2732–2734 (2013).
36. L. Diéguez, N. Darwish, M. Mir, E. Martínez, M. Moreno, and J. Samitier, "Effect of the refractive index of buffer solutions in evanescent optical biosensors," Sens. Lett. **7**(5), 851–855 (2009).